AD-A066 604 MISSION RESEARCH CORP SANTA BARBARA CALIF F/G 18/3
FIREBALL EFFECTS IN LATE-TIME EMP FROM SURFACE BURSTS.(U)
FEB 78 C L LONGMIRE, W E HOBBS DNA001-77-C-0135
UNCLASSIFIED MRC-R-249 DNA-4515T NL

1 OF 1
AD
A066604

END
DATE FILMED
5-79
DDC

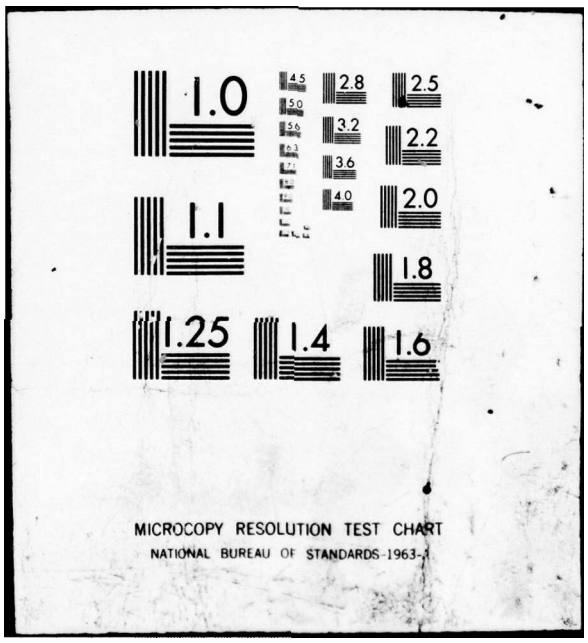
1.0
1.1
1.25
1.4
1.6
1.8
2.0
2.2
2.5
2.8
3.2
3.6
4.0
4.5
5.0
5.6
MICROCOPY RESOLUTION TEST CHART
NATIONAL BUREAU OF STANDARDS-1963-A

DNA 4515T

FIREBALL EFFECTS IN LATE-TIME EMP FROM SURFACE BURSTS

C. L. Longmire
W. E. Hobbs
Mission Research Corporation
735 State Street
Santa Barbara, California 93101

1 February 1978

Topical Report for Period 3 January 1977—1 February 1978

CONTRACT No. DNA 001-77-C-0135

THIS WORK SPONSORED BY THE DEFENSE NUCLEAR AGENCY
UNDER RDT&E RMSS CODE B323077464 R99QAXEA09172 H2590D.

Prepared for
Director
DEFENSE NUCLEAR AGENCY
Washington, D. C. 20305

Destroy this report when it is no longer needed. Do not return to sender.

PLEASE NOTIFY THE DEFENSE NUCLEAR AGENCY, ATTN: TISI, WASHINGTON, D.C. 20305, IF YOUR ADDRESS IS INCORRECT, IF YOU WISH TO BE DELETED FROM THE DISTRIBUTION LIST, OR IF THE ADDRESSEE IS NO LONGER EMPLOYED BY YOUR ORGANIZATION.

UNCLASSIFIED

SECURITY CLASSIFICATION OF THIS PAGE (When Data Entered)

REPORT DOCUMENTATION PAGE

READ INSTRUCTIONS BEFORE COMPLETING FORM

1. REPORT NUMBER: DNA 4515T
2. GOVT ACCESSION NO.
3. RECIPIENT'S CATALOG NUMBER

4. TITLE (and Subtitle): FIREBALL EFFECTS IN LATE-TIME EMP FROM SURFACE BURSTS.

5. TYPE OF REPORT & PERIOD COVERED: Topical Report. 3 Jan 77—1 Feb 78

6. PERFORMING ORG. REPORT NUMBER: MRC-R-249

7. AUTHOR(s): C. L. Longmire, W. E. Hobbs

8. CONTRACT OR GRANT NUMBER(s): DNA 001-77-C-0135

9. PERFORMING ORGANIZATION NAME AND ADDRESS
Mission Research Corporation
735 State Street
Santa Barbara, California 93101

10. PROGRAM ELEMENT, PROJECT, TASK AREA & WORK UNIT NUMBERS
NWED Subtask R99QAXE 172
A091

11. CONTROLLING OFFICE NAME AND ADDRESS
Director
Defense Nuclear Agency
Washington, D.C. 20305

12. REPORT DATE: 1 Feb 1978

13. NUMBER OF PAGES: 32

14. MONITORING AGENCY NAME & ADDRESS (if different from Controlling Office): 33 p.

15. SECURITY CLASS (of this report): UNCLASSIFIED

15a. DECLASSIFICATION/DOWNGRADING SCHEDULE

16. DISTRIBUTION STATEMENT (of this Report)

Approved for public release; distribution unlimited.

627044

17. DISTRIBUTION STATEMENT (of the abstract entered in Block 20, if different from Report)

18. SUPPLEMENTARY NOTES

This work sponsored by the Defense Nuclear Agency under RDT&E RMSS Code B323077464 R99QAXEA09172 H2590D.

19. KEY WORDS (Continue on reverse side if necessary and identify by block number)

Electromagnetic Pulse (EMP)
Nuclear Weapons Effects
Late-Time EMP
Close-In EMP
Conductivity Front
Magnetic Diffusion
Photodetachment
Blast Wave
Neutron Diffusion

20. ABSTRACT (Continue on reverse side if necessary and identify by block number)

This report describes the electrical properties of low altitude nuclear fireballs and discusses several effects of the fireball on the electromagnetic pulse (EMP) generated by nuclear explosion.

DD FORM 1 JAN 73 1473 EDITION OF 1 NOV 65 IS OBSOLETE

UNCLASSIFIED

SECURITY CLASSIFICATION OF THIS PAGE (When Data Entered)

406 548

78 12 20 011

PREFACE

The authors express gratitude to D. Sappenfield and R. Christian for many informative discussions during the course of this research.

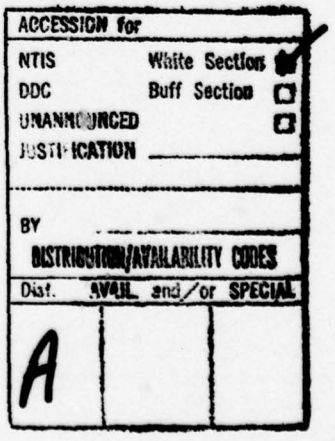

CONTENTS

SECTION 1
FIREBALL PROPERTIES AND SCALING

In this report we shall discuss some effects of the fireball and shock wave on the late-time EMP from a nuclear burst at the ground-air interface. We begin by describing some relevant properties of the fireball and their scaling with yield.

The nuclear energy is released, in a nuclear bomb, in times of the order of 10 ns. As a result of the high temperature and pressures developed within the bomb, the bomb materials explode with velocities of the order of 1 m/μsec. The expanding bomb materials pick up the air that lies in their path, and share their kinetic energy with it. In addition, a dominant fraction of the bomb energy flows out of the bomb in the form of thermal X rays, and is deposited in the air within a few meters from the bomb. The heated air in turn expands and re-radiates, sharing the energy with a still larger mass of air. There is a metric ton (10^3 kg) of air in a sphere of radius about 6 m. When the radius of the heated region is several times this value, the bomb mass is negligible compared with the air mass, and one expects the fireball to pass through a sequence of similar configurations, of which the length scale increases with time. At an early stage, for EMP interests, the spreading of energy becomes hydrodynamic rather than radiative; the hot air inside shares its energy with the cold air outside by driving a shock wave into the cold air, which is thereby heated to the same temperature as the air inside the shock wave.

The rate of growth of the fireball in the hydrodynamic phase, and the scaling with yield, can be understood from energy considerations.

Let v (m/sec) be the shock velocity. The average expansion velocity of the air within the fireball will be a constant fraction (not much less than unity) of v. Let R(m) and ρ_o(kg/m^3) be the radius of the shock wave and initial air density. Then, since the total kinetic energy in the fireball will be a constant fraction of the total yield Y (joules) (the remainder being internal energy of the hot air) we must have

$$\frac{1}{2}\left(\frac{4\pi}{3}R^3\right)\rho_o v^2 = kY \quad . \tag{1.1}$$

Here k is a combination of the two constant fractions invoked above, and depends on the equation of state of air. The value of k determined from detailed calculations is

$$k = 0.23 \quad . \tag{1.2}$$

Solving Equation 1.1 for v, which is dR/dt (t=time), we have

$$R^{3/2}\frac{dR}{dt} = \left(\frac{3}{2\pi}\frac{kY}{\rho_o}\right)^{1/2} \quad . \tag{1.3}$$

Integration of Equation 1.3 yields

$$\frac{2}{5}R^{5/2} = \left(\frac{3}{2\pi}\frac{kY}{\rho_o}\right)^{1/2} t$$

or

$$R = \left(\frac{5}{2}\right)^{2/5}\left(\frac{3}{2\pi}\frac{kY}{\rho_o}\right)^{1/5} t^{2/5} = 0.92\left(\frac{Y}{\rho_o}\right)^{0.2} t^{0.4} \text{ (mks units)}. \tag{1.4}$$

This formula is for a burst in free air. For a surface burst, the Y used in the formula should be twice the actual yield since the fireball is only a hemisphere and there is not much leakage of energy into the ground. Note that

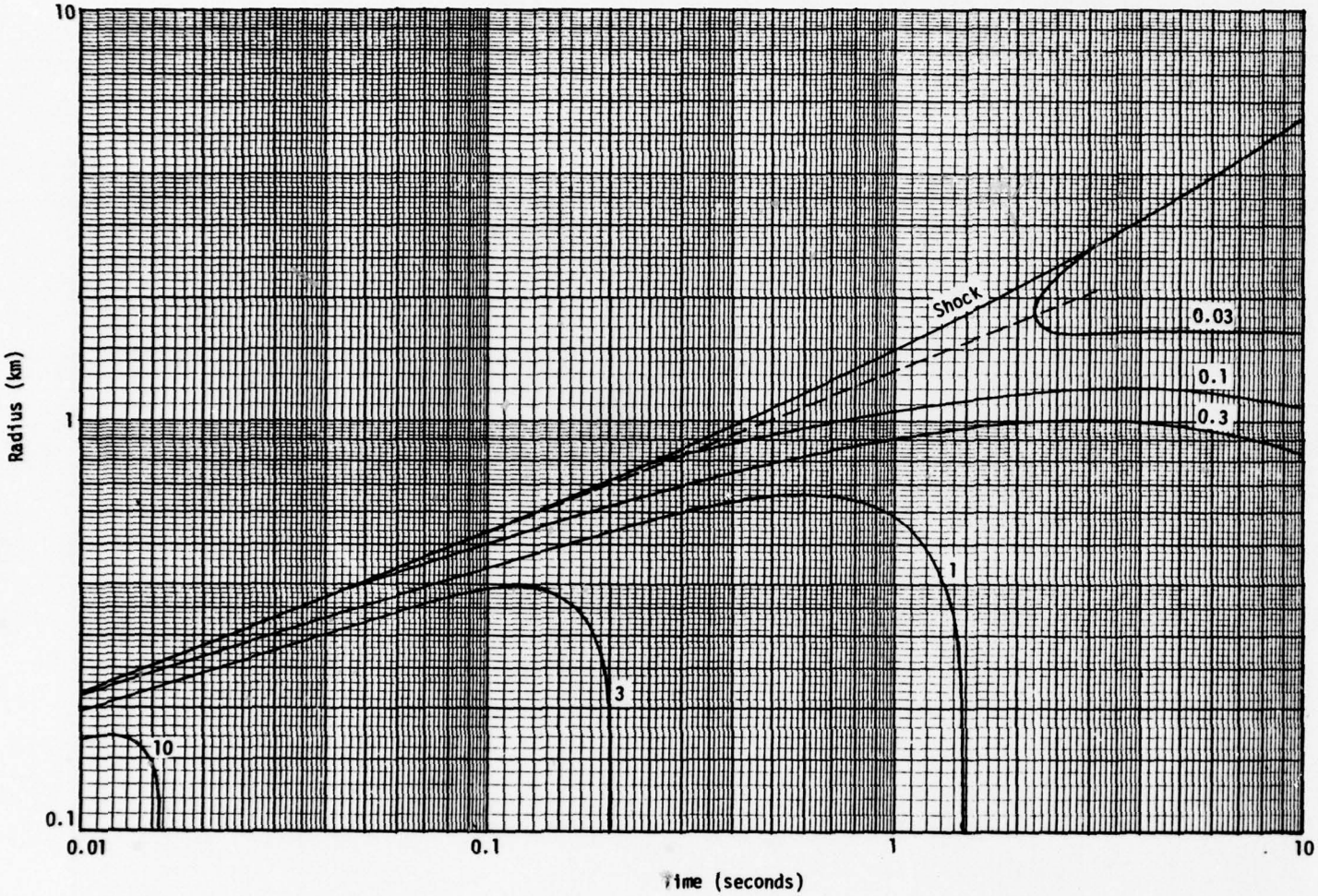

Figure 1. Contours of constant air temperature in radius-time plot for 1-megaton surface burst. The numbers near the curves are temperature in eV.

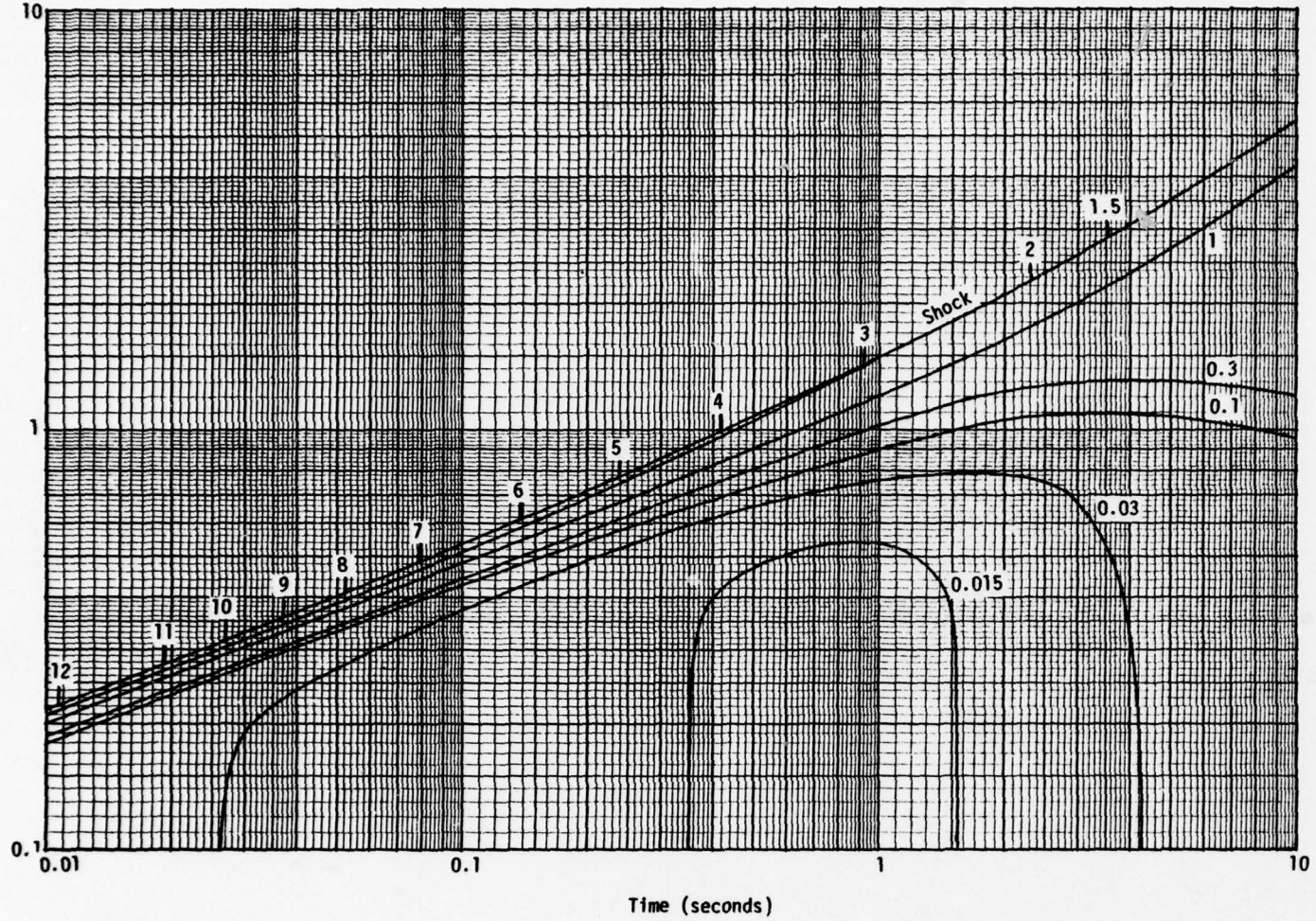

Figure 2. Contours of constant air density in radius-time plot for 1-megaton surface burst. Numbers indicate density relative to normal air density along shock front and on contours.

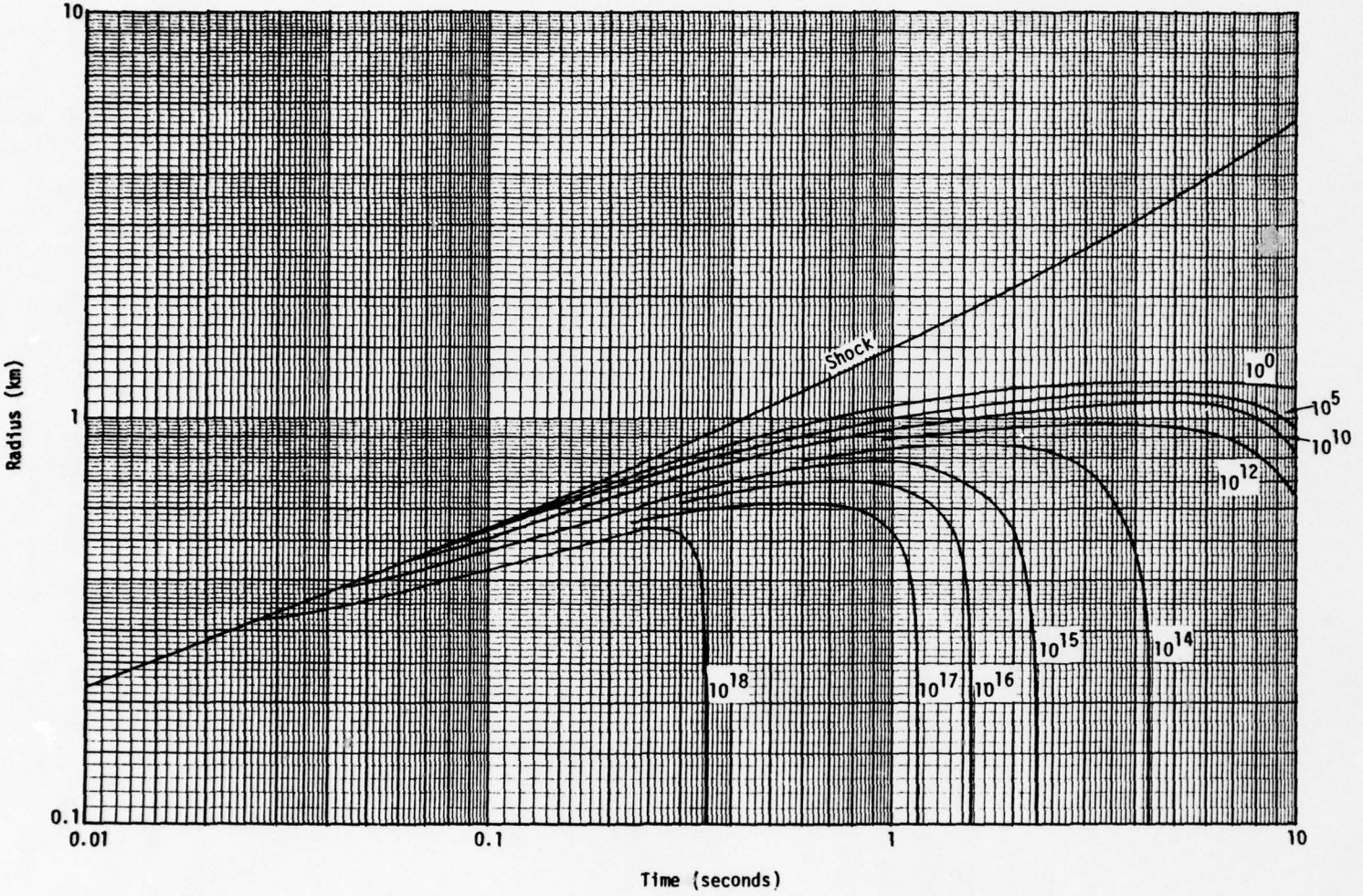

Figure 3. Contours of constant electron density in radius-time plot for 1-megaton surface burst. Numbers are electron density in electrons/cm^3.

$$1 \text{ megaton} = 4.18 \times 10^{15} \text{ joules} \tag{1.5}$$

$$\rho_o \approx 1.23 \text{ kg/m}^3 \quad \text{(near ground surface)} . \tag{1.6}$$

Figures 1, 2 and 3 show contours of temperature, relative mass density, and free electron density in radius-time plots for a 1 megaton surface burst (2 MT air burst). These results were computed by D. S. Sappenfield using his computer code RADFLO. The outermost contour is the shock wave radius versus time. The dashed curve in Figure 1 represents Equation 1.4, and we see that for times less than a few tenths of a second it is quite accurate. The calculation which led to Equation 1.4 neglected the thermal energy already in the air before the burst. At later times this energy is not negligible; for example, the shock velocity will not fall below the speed of sound in the ambient air. Thus Equation 1.4 loses accuracy at late times.

There is, however, an accurate scaling of Figures 1, 2 and 3 to other yields. For various yields Y, the ratio of bomb energy to ambient air energy in the fireball will be identical when the fireball radius R has a value such that R^3 is proportional to Y, or R is proportional to $Y^{1/3}$. Since the shock velocities in these cases will also be identical (Equation 1.1), the time (after burst) is also proportional to $Y^{1/3}$. Thus Figures 1, 2 and 3 apply to other yields if the time and distance scales are both changed as $Y^{1/3}$. For example, the figures would apply to 1 kiloton if the time "1 sec" were changed to read "0.1 sec" and the radius "1 km" were changed to read "0.1 km."

For the 1 MT case, the maximum radius of the fireball is about 1 km, although a weak shock wave travels outward to larger distances. The air within 1 km is left much hotter than ambient (1 eV = 11,606°K), and its mass density is much less than normal; the pressure is left at about 1 atmosphere. The electron densities in Figure 3 represent thermal ionization, and do not include ionization due to radioactivity. Thermal

ionization dominates inside the shock wave at early times, and inside about 1 km at later times. After a few seconds, the fireball rises off the ground due to its buoyancy; this effect is not included in the figures.

One can foresee several effects of the fireball on the EMP. First, the electrical conductivity will be high inside the fireball because of the free electrons. Thus, electric fields will be small there, and magnetic fields will tend to be pushed out by the expanding air. Second, outside the fireball proper, light from the fireball and heating by the shock wave tends to detach electrons from O_2^-, raising the conductivity. Finally, the reduced mass density in the fireball affects the source and transport of the late-time gammas. We shall estimate these effects in following sections of this report.

SECTION 2
MAGNETIC FIELDS WITH AN EXPANDING REGION OF HIGH CONDUCTIVITY

Once a gas begins to ionize, its conductivity increases rapidly with increasing temperature. In this section we review the basic mechanisms which govern the conductivity of a hot gas and apply them to our fireball. At early times ($t < 0.1$ sec) we find that a region of strong conductivity ($\gtrsim 1000$ mhos/m) will be travelling with the blast wave. This leads to a simple solution for the electromagnetic fields in the frame of the advancing front of high conductivity. We present this solution and briefly discuss its implications for an inner boundary condition for our EMP analysis.

FIREBALL CONDUCTIVITY

The conductivity σ of a hot, partially ionized gas is limited either by the electron collisions with neutrals or with other electrons. It is more straightforward to consider the resistivity which results from these processes since resistivities are additive; e.g.,

$$\sigma = (\eta_n + \eta_e)^{-1} \tag{2.1}$$

where η_n is the resistivity due to electron-neutral collisions and η_e is that due to charged-particle collisions.

The resistivity due to electron-neutral collisions may be read from a graph of Phelps.[1] Up to a temperature of 1 ev, this curve is approximately given by the formula,

$$\eta_n = 3.2 \times 10^{-6} \left(\frac{n_n}{n_e}\right) T^{0.7} \text{ (ohm-m)} \tag{2.2}$$

Here, n_e and n_n are electron and neutral particle densities and T is the temperature in electron volts. Above approximately 1 ev, air becomes strongly ionized $(n_n \to o)$ and at the higher temperatures the resistivity is dominated by charged-particle collisions.

Due to the long-range nature of the Coulomb force the resistivity of an electron gas is enhanced due to the multitude of small angle collisions. The theory for the resistivity of a singly ionized gas was first developed by Landshoff[2] and a later analysis by Spitzer and Harm[3] is in full agreement; their formula is

$$\eta_e = 5.2 \times 10^{-5} \frac{\ln\Lambda}{T^{3/2}} \text{ (ohm-m)} \qquad (2.3)$$

with T again in electron volts. The Coulomb logarithm $\ln\Lambda$ in this expression is a slowly varying function of electron temperature and density. It is well approximated by the value 10 for conditions for which we are interested.

The information of Figures 1, 2 and 3 may be used to calculate the conductivity as given by Equation 2.1 using Equations 2.2 and 2.3. The neutral particle density is found using $n_n = \mu n_o$ where μ is the relative air density from Figure 2, and n_o is the quiescent particle density $n_o = 5 \times 10^{19}$. Figure 4 summarizes our calculations. The charged-particle collisions are the limiting mechanism for conductivities greater than about 1000 mhos/m.

MAGNETIC FIELD PROFILES ACROSS THE SHOCK

For our one megaton model problem, very high conductivity exists in the fireball. At the earlier times this conductivity is turned on in the shock front, while the air is being compressed. The question arises as to whether the magnetic field swept over by the shock is compressed along with the air in the shock. We shall see that it is not.

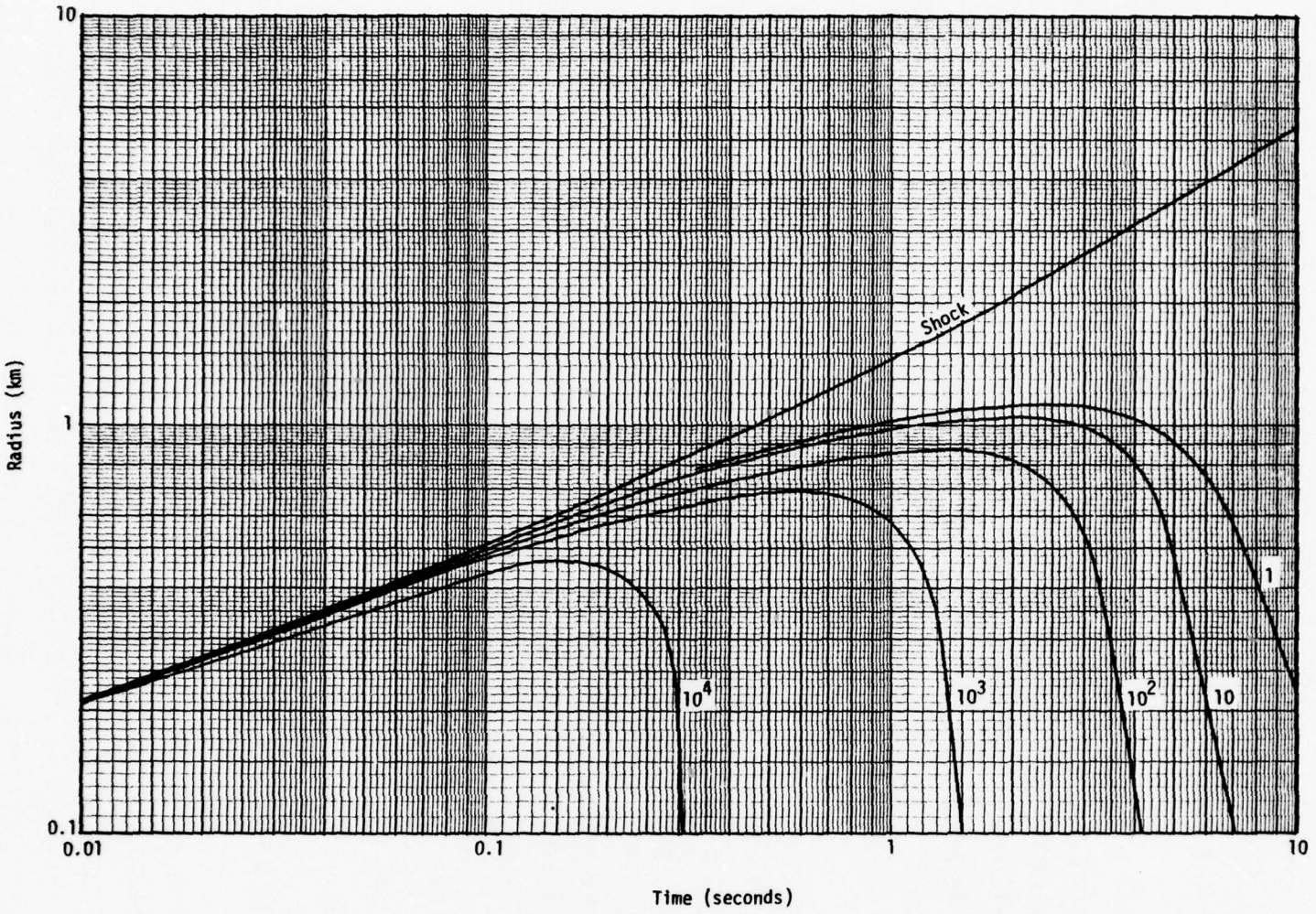

Figure 4. Contours of constant electrical conductivity in radius-time plot for 1-megaton surface burst. The numbers near the curves are conductivity in mhos/m.

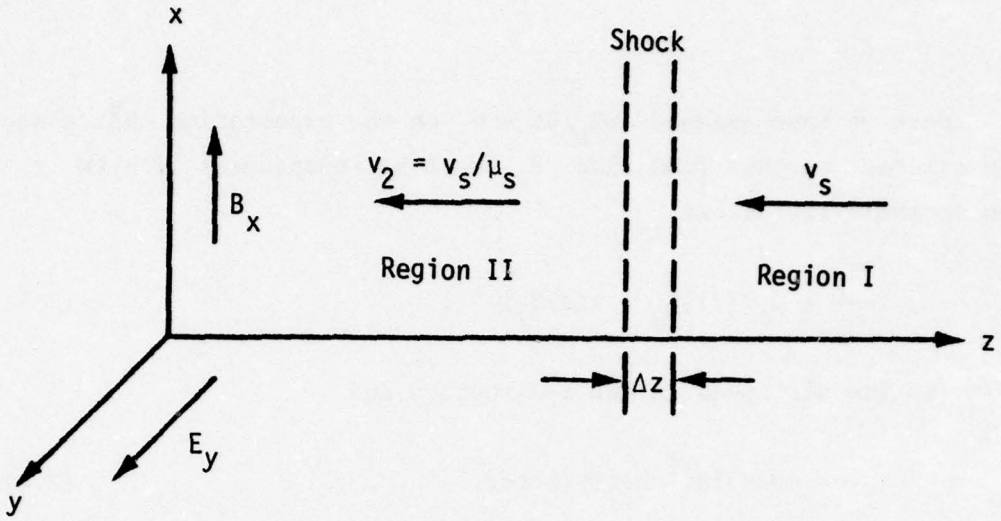

Figure 5. Electric and magnetic fields—shock geometry.

Let us consider the one-dimensional flow problem sketched in Figure 5 above. Air flows from right to left, being at ambient density and temperature in Region I, where it is not highly conducting. The shock structure is contained between the two planes Δz apart; within this region the air is compressed, heated, and made conducting. The shock is at rest in our coordinate system; it would move to the right with speed v_s if Region I were brought to rest (lab. system). In Region II the air density is greater than ambient by the compression ratio μ_s, and the air speed is reduced by a factor μ_s, to conserve mass. The conductivity is high in Region II. In Region I we have an initial magnetic field B_1 in the x-direction. What is the magnetic field in Region II?

Any change in the magnetic field will induce an electric field in the y-direction. One relation between the electric and magnetic fields is Faraday's law,

$$\frac{\partial E_y}{\partial z} = \frac{\partial B_x}{\partial t} = 0 \quad . \tag{2.4}$$

Here we have assumed $\partial B_x/\partial t = 0$ on the expectation that a steady solution exists. We thus find that E_y must be independent of both z and t. Then Ampere's law becomes

$$\frac{\partial B_x}{\partial z} = \mu_o \sigma(z)[E_y - v(z)B_x] \quad , \tag{2.5}$$

where $-v$ is the air speed in the z-direction and

$$\mu_o = 4\pi \times 10^{-7} \text{ henry/meter.} \tag{2.6}$$

We have used here Ohm's law for a moving medium. In Region II, where σ and v are constant, the general solution of Equation 2.5 is

$$B_x = \frac{E_y}{v_2} + A \exp(-\mu_o \sigma v_2 z) \quad . \tag{2.7}$$

Here A is an arbitrary constant, but since we want our solution to be well-behaved as $z \to -\infty$, we must choose $A = 0$. Thus we must have, in Region II,

$$v_2 B_2 = E_y \quad . \tag{2.8}$$

Now, let us see whether B_x can change appreciably within the shock structure. From Equation 2.5 we can estimate the change ΔB_x across the shock as

$$\frac{\Delta B_x}{B_x} \approx -\mu_o \sigma v \Delta z \quad . \tag{2.9}$$

In order not to underestimate ΔB_x we use the maximum value of σ, i.e. that behind the shock, and the maximum value v_s of v. From Figure 4 we choose

$$\sigma = 10^3 \text{ mho/m}$$

$$v = 6 \times 10^3 \text{ m/s} \quad .$$

The shock thickness is certainly less than 1 mm. Thus, we find

$$\frac{\Delta B_x}{B_x} < (4\pi \times 10^{-7})(10^3)(6 \times 10^3)(10^{-3}) \\ < 0.0075 \quad . \tag{2.10}$$

We see that the change in B_x across the shock structure itself is negligible.

In region I, a solution similar to Equation 2.7 holds. However, the air here is only weakly conducting because of gamma induced ionization. The relaxation length $(\mu_o \sigma v_s)^{-1}$ tends to be very long here, so that in our one dimensional problem B_x is approximately constant, and

$$B_1 \approx B_2 \quad . \tag{2.11}$$

In the actual EMP problem, the fall-off of B in the region outside the fireball is determined by the fall-off of the Compton current source.

We can derive a boundary condition to use in the EMP calculation at the fireball radius. This boundary condition relates E_θ and B_ϕ (in terms of spherical coordinates). In the shock frame this condition is just Equation 2.8, which in the Gaussian units used in LEMP and SUBL reads

$$E'_\theta = -\frac{v_2}{c} B_\phi = -\frac{v_s}{\mu_s c} B_\phi \quad . \tag{2.12}$$

In the laboratory (or LEMP-SUBL) system

$$E_\theta = E'_\theta + \frac{v_s}{c} B_\phi = \left(1 - \frac{1}{\mu_s}\right) \frac{v_s}{c} B_\phi \quad . \tag{2.13}$$

This equation says that the air behind the shock is regarded as a perfect conductor. If we drop the term $1/\mu_s$ as being small compared with unity, the result is equivalent to assuming that the shock front itself is a moving perfect conductor. There is no strong reason to choose one of these models over the other. If we drop $1/\mu_s$, there will be no magnetic flux inside the shock. If we retain it, the magnetic field just behind the shock will be the same as that just ahead of the shock, but the magnetic field will be very low in that part of the fireball where the air density is very low.

It is simpler in SUBL to drop the $1/\mu_s$ term, since then it is not necessary to solve Maxwell's equations inside the fireball. For this reason, we shall adopt this procedure in modifying SUBL. In this case we need only to specify the shock position (or speed) as a function of time, and do not need to describe the air motions inside the shock.

SECTION 3
EFFECT OF FIREBALL ON GEOMAGNETIC FIELD

The geomagnetic field is not included in LEMP and SUBL calculations, since additional field components and (in general) 3-D calculations would be required. However, we can now easily estimate the magnitude of the MHD effects involving the geomagnetic field.

We saw, in Section 2, that the geomagnetic field will be almost entirely pushed out of the fireball because the compression in the shock front occurs in such a short distance that the magnetic field cannot be compressed with the air. As the air is compressed most of the magnetic field "squirts out" into the low conductivity region ahead of the shock. According to Equation 2.13, only a fraction $1/\mu_s$ of the flux swept over is retained in the compressed air. We shall ignore this small fraction and drop the $1/\mu_s$ term. Then all of the field is pushed out of the fireball. There will be no geomagnetic field inside the fireball, and outside there will be a dipole field superposed upon a uniform field. (The air conductivity outside the fireball is small by the time ($t>0.01$ sec) the fireball effects are of interest; magnetic relaxation times in the ground are also short compared with these times of interest.)

For a complete spherical fireball, the maximum geomagnetic field on its surface would be 3/2 of the ambient field. For the hemispherical fireball this value is not quite right, but we can use it for an estimate. For a vertical geomagnetic field B_o we would then have an azimuthal electric field E_ϕ at the ground surface given by

$$E_\phi \approx \frac{3}{2} \frac{v_s}{c} B_o \quad . \tag{3.1}$$

Evaluating this estimate for

$$v_s = 6 \times 10^3 \text{ m/s (at } t \approx 0.01 \text{ sec)} \quad ,$$

$$B_o = 0.6 \text{ gauss} \quad ,$$

we obtain

$$\begin{aligned} E_\phi &\approx 1.8 \times 10^{-5} \text{ esu} \\ &= 0.54 \text{ v/m} \quad . \end{aligned} \tag{3.2}$$

This result holds at the fireball radius. At larger distances E_ϕ falls off as $1/r^2$.

E_ϕ also falls off as time increases because the shock speed decreases. Eventually, the conductivity of the fireball becomes so low that the geomagnetic field diffuses back into it. The distance diffused (or skin depth) at time t is

$$\delta \approx \sqrt{\frac{2t}{\mu_o \sigma}} \tag{3.3}$$

Putting $\delta = 10^3$ m (the maximum fireball radius for 1 megaton) we find the diffusion time to be

$$\begin{aligned} t &\approx 0.6\sigma \\ &\approx 6 \text{ seconds, if } \sigma = 10 \text{ mho/m} \end{aligned} \tag{3.4}$$

From Figure 4 we see that the conductivity is indeed about 10 mho/m at six seconds, so that this is the time when the field will diffuse back into the fireball. By this time the fireball has risen appreciably.

SECTION 4
NEUTRON DIFFUSION ACROSS A SHOCK

Neutron capture by nitrogen nuclei is the major source of late-time gamma rays in close-in EMP calculations. In this section we will discuss the effect of the blast wave on the spatial and temporal distribution of these sources.

The prompt neutrons produced in the detonation initially have an energy of the order of an Mev and the cross section for the elastic scattering of these neutrons by air nuclei is a few barns. The neutrons will therefore have a high collision frequency ($\sim 10^5$ sec^{-1}) and will thermalize before the arrival of the blast wave. The blast wave will expand with velocities of the order of the sound velocity and will arrive at a given radius somewhat after the neutrons.

The blast wave will tend to sweep up the air as it proceeds outward. The result is a shell ($\sim$10-20 m. thick) of dense air following the shock front. By continuity the shell must be relatively hollow; i.e., the air within the shell is rarefied. The dense shell of air will itself tend to collect the neutrons as it proceeds outward and, to first order, this process is examined using diffusion theory.

In the derivation of the neutron diffusion equation the scattering centers are assumed to be at rest in the laboratory frame of reference. If the scattering centers have a flow velocity, the diffusion equation must be modified to account for this. Let $\vec{F}'$ be the neutron flux in the frame of the moving medium and $\vec{u}$ be the velocity of this medium relative to an observer's frame. If $\vec{F}$ and n are the flux and density in the

observer's frame, then it is straightforward to show that

$$\vec{F} = \vec{F}' + \vec{un} \quad . \tag{4.1}$$

Fick's law for the neutron flux in the moving frame is given as usual,

$$\vec{F}' = - \frac{\lambda \langle v \rangle}{3} \nabla n \tag{4.2}$$

where λ is the transport mean-free path and $\langle v \rangle$ is the characteristic neutron velocity. The neutron velocity distribution is assumed to be sharply peaked about this velocity; i.e., we are using one-velocity diffusion theory.

The flux in the observer's frame is therefore expressed as

$$\vec{F} = - \frac{\lambda \langle v \rangle}{3} \nabla n + \vec{un} \quad . \tag{4.3}$$

Substituting this into the continuity equation yields our Galilean-transformed diffusion equation

$$\frac{\partial n}{\partial t} = - \nabla \cdot \vec{F} = \nabla \cdot \left(\frac{\lambda \langle v \rangle}{3} \nabla n - \vec{un} \right) \quad . \tag{4.4}$$

The value of the diffusion coefficient in this equation $\lambda \langle v \rangle / 3$ is approximately 4×10^8 cm^2/sec. The diffusion times are short compared with the hydrodynamic times and the neutron density will quickly relax to a quasi-static profile in the frame of the blast wave. The stationary profile is found by solving the diffusion equation with the time derivatives neglected.

As in Section II, the geometry is such that the curvature of the fireball is negligible and a one-dimensional analysis is applicable. Equation 4.4 then yields, on integrating once with respect to x,

$$\frac{\lambda \langle v \rangle}{3} \frac{\partial n}{\partial x} - un = -v_s n_o \quad . \tag{4.5}$$

The constant of integration is evaluated by assuming that at some distance in front of the shock the neutron density is a constant n_o; v_s is again the shock velocity.

The neutron transport mean-free path λ is inversely proportional to the density which is a function of position. In the frame of the shock there will be hydrodynamic equilibrium with the material flux ρu constant. Equation 4.5 may therefore be rewritten

$$\kappa \frac{\partial n}{\partial x} - n = \frac{-v_s n_o}{u(x)} \tag{4.6}$$

where $\kappa = \frac{\lambda \langle v \rangle}{3u} \propto \frac{1}{\rho u}$ is the constant characteristic scale length for the change in neutron density. It is a simple matter to solve this equation for arbitrary shock profiles.

As a model we consider the three region one-dimensional situation shown in Figure 6. The dashed lines indicate the air density in the frame of the shock. Region 1 is the ambient medium in front of the shock. The shock front is at x_s behind which is the dense shell Region 2. To the left of the origin is the rarefied core Region 3. For these regions of constant density the solutions of Equation 4.6 are readily obtained,

$$n = A_i + B_i \exp(-x/\kappa) \tag{4.7}$$

where the subscripts specify a region. The particular solution is given by $A_i = n_o v_s / u_i$ where the u's are known since the air flux ρu is constant. The B's are evaluated by applying neutron density continuity at the interfaces and the fact the neutron density must be bounded.

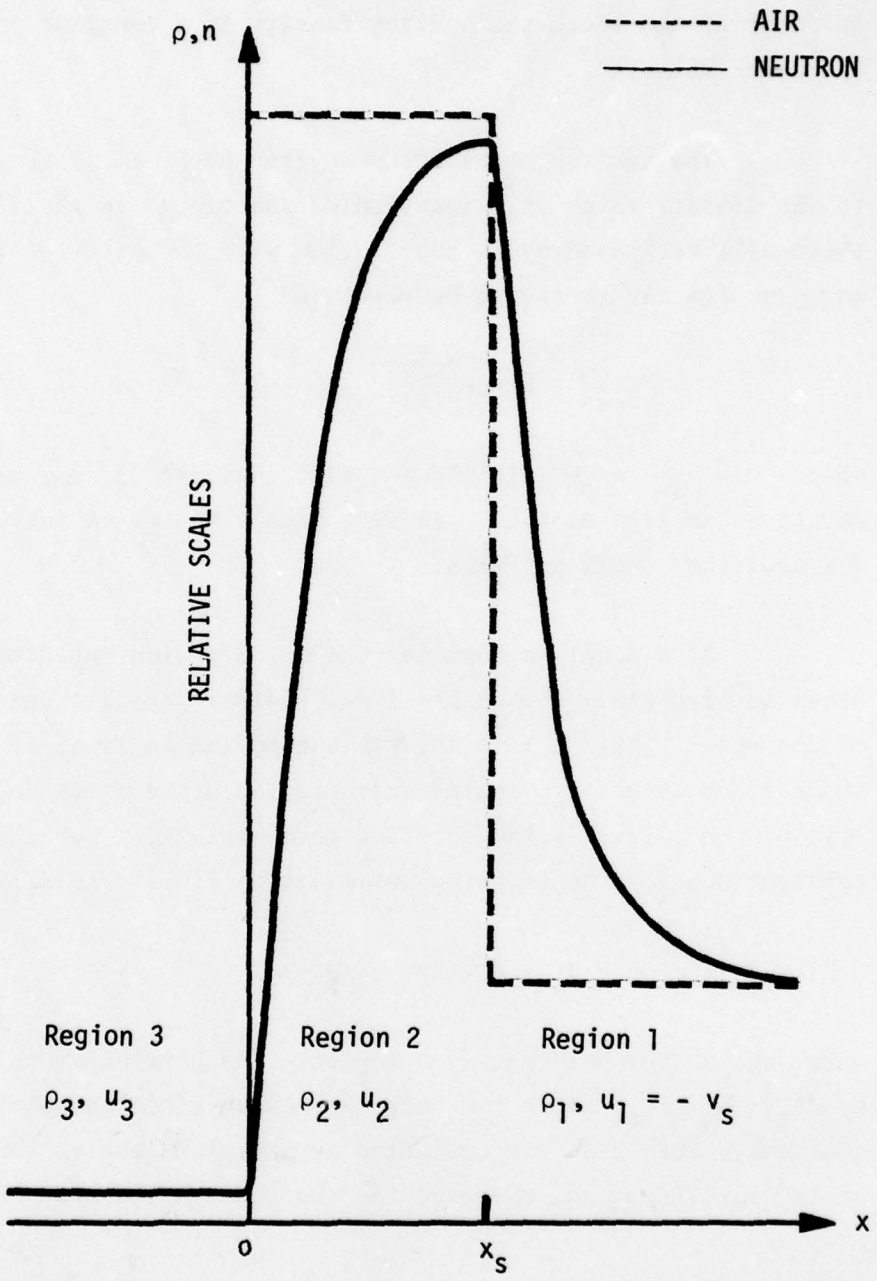

Figure 6. Blast-wave air and neutron densities.

$$n = \begin{cases} n_o \left[1 + \dfrac{(\rho_2-\rho_1)\exp(x_s/\kappa) + (\rho_3-\rho_2)}{\rho_1} \exp(-x/\kappa) \right] & x_s<x \\ n_o \left[\dfrac{\rho_2 + (\rho_3-\rho_2)\exp(-x/\kappa)}{\rho_1} \right] & o<x<x_s \\ n_o \left(\dfrac{\rho_3}{\rho_1} \right) & x<o \end{cases} \qquad (4.8)$$

In Figure 6 we have included the curve for the neutron density for the case when $\rho_2/\rho_1 = 6$, $\rho_3/\rho_1 = 0.1$ and $x_s/\kappa = 4$. These parameters represent a typical shock for the 1-megaton surface burst at 0.1 second (see Figure 1).

In LEMP and SUBL we currently use a neutron-capture gamma source which assumes constant air density. It utilizes numerical fits of the monte-carlo calculations of Sargis, et al.[4] It is a straightforward matter to incorporate the above results into the time history of our late-time gamma sources.

We have air density profiles as a function of time. Figure 2 gives this information in detail but parameterized profiles like Figure 6 are sufficiently accurate in this analysis. We know the total time-integrated number of neutrons to be absorbed; it is the same as that when the blast wave was ignored. This gives us the initial number of neutrons. We can then calculate the neutron density profile as was done above, and calculate the number of neutrons absorbed and the number of gammas produced in a time step. Subtracting the neutrons captured gives the number for the new air density profile of the next time step. The process is repeated for the duration of the EMP calculation. In calculating neutron loss due to capture, both processes which contribute to the depletion of thermal neutrons in air are included. The larger cross section (~1.7 b) is for the (n,p)

reaction which produces C^{14}. The one of interest in EMP computations is the less common (n,γ) reaction ($\sim$0.1 b) which produces a 6 Mev gamma ray.

After the detonation the prompt neutrons will establish their spatial distribution rapidly (on the order of a few milliseconds). After the neutrons have thermalized they essentially come to a halt relative to the velocity of the blast. The nitrogen-capture gamma-source region has a radius of about 200 m. The mean time to capture for thermal neutrons in standard-temperature-and-pressure air is about 0.06 sec. Except for small yields ($\lesssim$20 kilotons), the blast wave will completely engulf the neutron spatial distribution within this time. Once this occurs the neutrons will be more slowly absorbed in the tenuous core of the fireball.

In general, due to the enhanced densities, we will initially obtain a stronger gamma source. Later, after the fireball engulfs the neutrons, the source will be somewhat weaker but more persistent. The details of how the model outlined here is incorporated in the SUBL code will be described in a later report.

SECTION 5
PHOTODETACHMENT OF O_2^- .

The radiation from the fireball is that of a blackbody with a temperature of several thousand degrees. Even though this radiation is very intense near the fireball, we will show in this section that it will result in a negligible number of electrons being detached from the O_2^- .

The sun also emits blackbody radiation with a temperature of several thousand degrees. The photodetachment rate for O_2^- in sunlight[5] has been found to be 0.3 sec^{-1}. The radiation from the fireball will have about the same spectrum but will, of course, be much more intense close-in where the EMP is produced. We can find an upper limit on the O_2^- destruction rate by multiplying the rate at the earth by the square of the ratio of distance to the sun to the sun's radius. We find a detachment rate of 1.5×10^4 sec^{-1}. This would be at the surface of the sun and corresponds to the detachment rate near the surface of the fireball. The destruction rates at some distance away from the fireball would be smaller. In contrast, the electron-oxygen attachment rates are of the order of 10^8 sec^{-1} for typical conditions. Since the ratio of electron mobility to ion mobility is about 10^3, we can ignore the effect of photodetachment caused by light from the fireball.

After a period of time the hydrodynamic shock wave will separate from the cooling fireball. This may be discerned from an examination of Figure 1. This separation will occur somewhat after the times of interest to EMP, at about 0.3 second in Figure 1. Only a thin region outside the fireball is heated sufficiently by this weaker shock to detach the electrons.

SECTION 6
SUMMARY

We have presented in Figures 1 through 4 a set of yield-scalable fireball characteristics of importance for EMP effects at late times. We have developed in Section 2 a simple way of including the effect of the shock wave and fireball conductivity in EMP calculations such as SUBL. In Section 3 we have made estimates of the electric field due to interaction of the fireball with the geomagnetic field. The estimated field is small (~500 volts/km), but could be important for wires or wire loops with dimensions of the order of several kilometers. In Section 4 we have constructed a model of the effect of the blast wave and fireball rarefaction on the neutron capture gamma source, which also can be put into SUBL. In Section 5 we have shown that the effect of photodetachment due to fireball light is negligible for EMP purposes.

REFERENCES

1. Phelps, A. V., Private Communication; A. G. Englehardt, A. V. Phelps, and C. G. Rick, Phys. Rev., 135, 1566 (1964).

2. Landshoff, R., Phys. Rev., 76, 904 (1949).

3. Spitzer, L., and R. Harm, Phys. Rev., 89, 977 (1953).

4. Sargis, D. A., Late-Time Sources for Close-In EMP, Science Applications, Inc., SAI-72-556-LJ, DNA 3064F, August 1972.

5. Burch, D. S., S. J. Smith, and L. M. Branscomb, Phys. Rev., 112, 171 (1958); ibid. 114, 1652 (1959).

DISTRIBUTION LIST

DEPARTMENT OF DEFENSE

Assistant to the Secretary of Defense
Atomic Energy
ATTN: Executive Assistant

Defense Civil Preparedness Agency
Assistant Director for Research
ATTN: TS AED

Defense Communication Engineer Center
ATTN: Code R720, C. Stansberry

Defense Communications Agency
ATTN: CCTC, C312
ATTN: Code C313

Defense Documentation Center
Cameron Station
12 cy ATTN: DD

Defense Nuclear Agency
ATTN: RAEV
ATTN: DDST
4 cy ATTN: TITL

Field Command
Defense Nuclear Agency
ATTN: FCPR

Interservice Nuclear Weapons School
ATTN: TTV

Joint Strat. Tgt. Planning Staff
ATTN: JSAS
ATTN: JPST

Livermore Division, Fld. Command, DNA
Lawrence Livermore Laboratory
ATTN: FCPRL

National Security Agency
ATTN: S232, D. Vincent

Under Secy. of Def. for Rsch. & Engrg.
ATTN: Strategic & Space Systems (OS)

Commandant
NATO School (SHAPE)
ATTN: U.S. Documents Officer

DEPARTMENT OF THE ARMY

Eradcom. Technical Support Activity
ATTN: DELET-IR, E. Hunter
ATTN: DRDCO-COM-ME, G. Gaule
ATTN: DRDCO-COM-ME

Harry Diamond Laboratories
ATTN: DELHD-N-EM
ATTN: DELHD-N-EMC, T. Wyatt
ATTN: DELHD-N-RBA
ATTN: DELHD-N-NP
ATTN: DELHD-N-RBC

DEPARTMENT OF THE ARMY (Continued)

U.S. Army Ballistic Research Labs.
ATTN: DRXBR-AM, W. VanAntwerp

U.S. Army Comm-Elec. Engrg. Instal. Agency
ATTN: CCC-CED-SES

U.S. Army Electronics Rsch. & Dev. Command
ATTN: DRCPM-ATC

U.S. Army Intelligence & Sec. Cmd.
ATTN: Technical Information Facility

DEPARTMENT OF THE NAVY

Civil Engineering Laboratory
Naval Construction Battalion Center
ATTN: Code L08A

Naval Ocean Systems Center
ATTN: Code 015, C. Fletcher

Naval Research Laboratory
ATTN: Code 6623, R. Statler
ATTN: Code 4104, E. Brancato

Naval Surface Weapons Center
ATTN: Code F31

Naval Surface Weapons Center
Dahlgren Laboratory
ATTN: Code DF-56

Naval Weapons Evaluation Facility
ATTN: Code AT-6

Strategic Systems Project Office
ATTN: NSP-230, D. Gold
ATTN: NSP-2342, R. Coleman
ATTN: NSP-27334

DEPARTMENT OF THE AIR FORCE

Aeronautical Systems Division, AFSC
ATTN: ASD-YH-EX

Air Force Technical Applications Center
ATTN: TFS, M. Schneider

Air Force Weapons Laboratory
ATTN: ELT, W. Page
ATTN: SUL
ATTN: NXS
ATTN: NTN

Foreign Technology Division, AFSC
ATTN: NICD, Library

Sacramento Air Logistics Center
ATTN: MMSREM, F. Spear
ATTN: MMCRS, H. Pelmastro
ATTN: MMIRA, J. Demes

DEPARTMENT OF ENERGY

Albuquerque Operations Office
ATTN: Operational Safety Div.

DEPARTMENT OF DEFENSE CONTRACTORS

Aerospace Corp.
ATTN: C. Greenhow

Bendix Corp.
Research Laboratories Division
ATTN: M. Frank

Bendix Corp.
Navigation and Control Group
ATTN: Dept. 6401

Boeing Co.
ATTN: H. Wicklein

Computer Sciences Corp.
ATTN: R. Dickhaut

Dikewood Industries, Inc.
ATTN: K. Lee

Fairchild Camera and Instrument Corp.
ATTN: D. Myers

Franklin Institute
ATTN: R. Thompson

General Electric Co.
Aerospace Electronics Systems
ATTN: C. Hewison

General Electric Co.
ATTN: Technical Library

General Electric Co.-TEMPO
Alexandria Office
ATTN: DASIAC

General Research Corp.
3 cy ATTN: Technical Information Office

Georgia Institute of Technology
Office of Contract Administration
ATTN: Res. & Sec. Coord. for H. Denny

GTE Sylvania, Inc.
Electronics Systems Grp.-Eastern Div.
ATTN: L. Blaisdell

Hazeltine Corp.
ATTN: M. Waite

Hughes Aircraft Co.
ATTN: K. Walker

IIT Research Institute
Electromag. Compatability Anal. Ctr.
ATTN: ACOAT

International Tel. & Telegraph Corp.
ATTN: A. Richardson

DEPARTMENT OF DEFENSE CONTRACTORS (Continued)

Kaman Sciences Corp.
ATTN: J. Lubell

University of California
Lawrence Livermore Laboratory
ATTN: Doc. Con. for L-156, E. Miller
ATTN: Doc. Con. for L-545, D. Meeker

Lockheed Missiles & Space Co., Inc.
ATTN: M. Bernstein
ATTN: B. Kimura

Los Alamos Scientific Laboratory
ATTN: Doc. Con. for B. Noel

Mission Research Corp.
ATTN: W. Hobbs
2 cy ATTN: C. Longmire
5 cy ATTN: Document Control

Northrop Corp. Electronic Division
ATTN: Rad. Effects Grp.

R & D Associates
ATTN: M. Grover
ATTN: C. MacDonald

R & D Associates
ATTN: J. Bombardt

Rand Corp.
ATTN: W. Sollfrey

RCA Corp.
ATTN: R. Rostrom

Rockwell International Corp.
ATTN: N. Rudie

Sanders Associates, Inc.
ATTN: R. Despathy, Sr.

Sandia Laboratories
ATTN: Doc. Con. for E. Hartman
ATTN: Doc. Con. for C. Vittitoe

Science Applications, Inc.
ATTN: N. Byrn

Sperry Rand Corp.
ATTN: M. Cort

Spire Corp.
ATTN: J. Uglum

Systems, Science & Software, Inc.
ATTN: A. Wilson

TRW Defense & Space Sys. Group
ATTN: R. Plebuch
ATTN: W. Gargaro
ATTN: H. Holloway

United Technologies Corp.
ATTN: Chief Elec. Design